Supplementary Material to: Quantifying Rotation-Induced Errors in Near-Field Seismic Recordings: Assessing Impact on Rotation and Acceleration Measurements.

Yara Rossi * [1,2], **Felix Bernauer** [1], **Chin-Jen Lin** [3], **Frédéric Guattari** [4], **Baptiste Pinot** [5]

[1]Department of Earth and Environmental Sciences, Ludwig-Maximilians Universität in München, Munich, Germany, [2]Department of Earth Sciences, University of Oregon, Eugene, USA, [3]Institute of Earth Sciences, Academia Sinica, Taipei, Taiwan, [4]MAÅGM, Le Mans, France, [5]Institut Supérieur de l'Aéronautique et de l'Espace (ISAE-SUPAERO), Toulouse, France

1 Additional Figures

The Figures presented in the Supplementary materials show the timeseries for each event discussed in the main text. Figure 1 and in Figure 2 show the highpass and lowpass filtered timeseries of the Ml 3.18 earthquake recorded at UWE station at the Kīlauea Caldera. Figure 3 and in Figure 4 show the highpass and lowpass filtered timeseries of the Ml 4.36 recorded at UWE station at the Kīlauea Caldera. Even for these earthquakes with a small magnitude, a permanent rotation of the station is visible. There is a visible difference between the demeaned and rotation corrected accelerations, that also translates to the displacements. Unfortunately, the displacements cannot be recovered nicely with either method for either earthquake.

The summit collapses at the Kīlauea Caldera show surprising similarities in the wave forms, as can be seen in Figure 5 (highpass) and in Figure 6 (lowpass) for the collapse on 2018/07/13 compared to Figure 7 (highpass) and in Figure 8 (lowpass) for the collapse on 2018/07/14.

The Mw 7.4 earthquake in Hualien, Taiwan on 2024/04/02 was recorded by two 6C-stations encompassing each an accelerometer and a rotational sensor. The time series of the station MDSA0 is shown in Figure 9 (highpass) and in Figure 10 (lowpass). For station NA01 the timeseries are shown in Figure 11 (highpass) and in Figure 12 (lowpass). Comparing the two stations, it is evident that they display very different wave forms, unsurprisingly, as they are located on different rupture fault patches.

*Corresponding author: rossi.yara@outlook.com

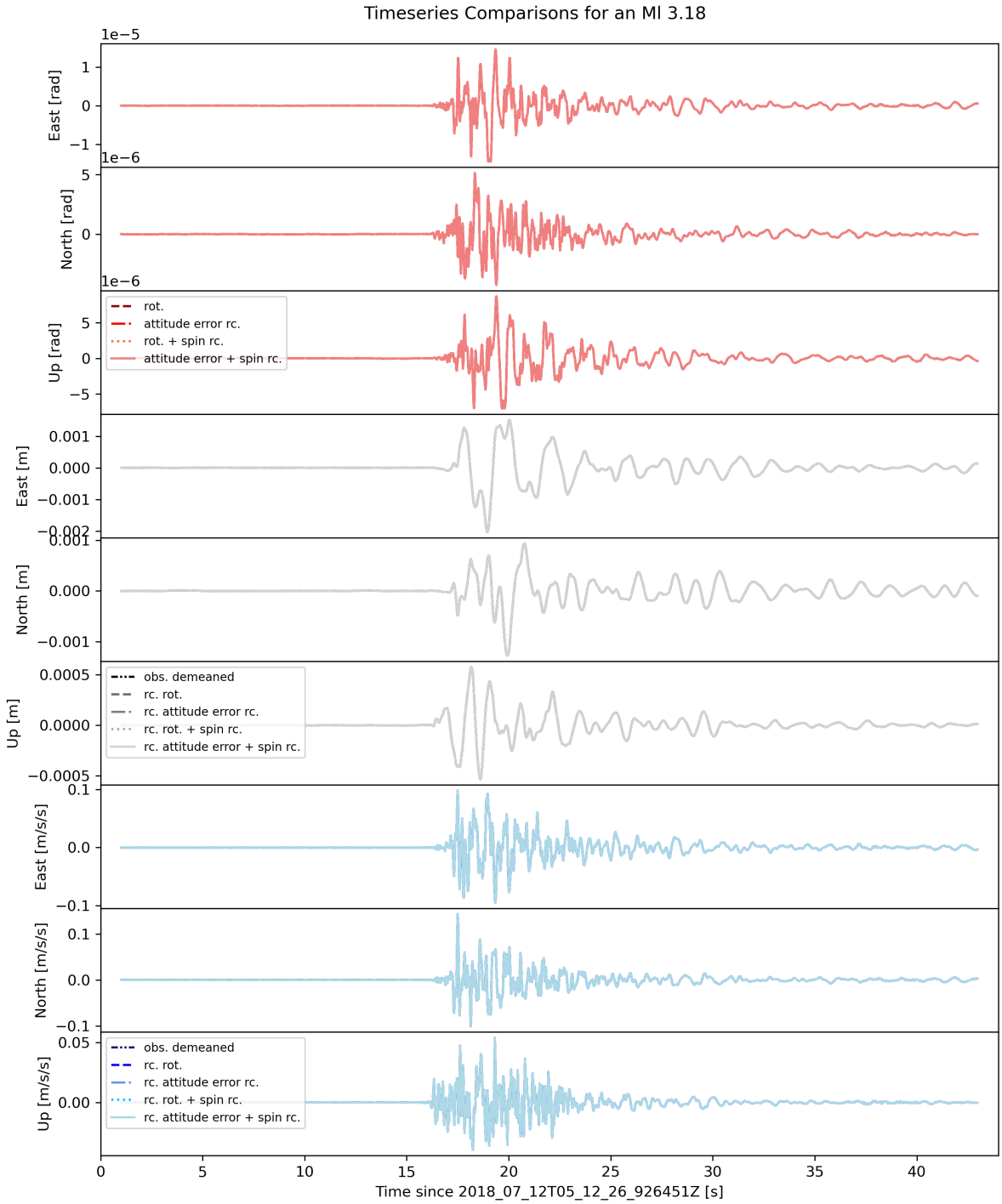

Figure 1 Recording of an earthquake with an Ml 3.18 at Kīlauea Caldera on 2018/07/12 using a highpass filter. Top subfigures show the timeseries of the four versions of the angles; uncorrected and three rotation corrected versions. The middle subfigures show the displacement applying either demeaning or rotation correction using each of the four angles from above. The lowest subfigures show the same but for acceleration.

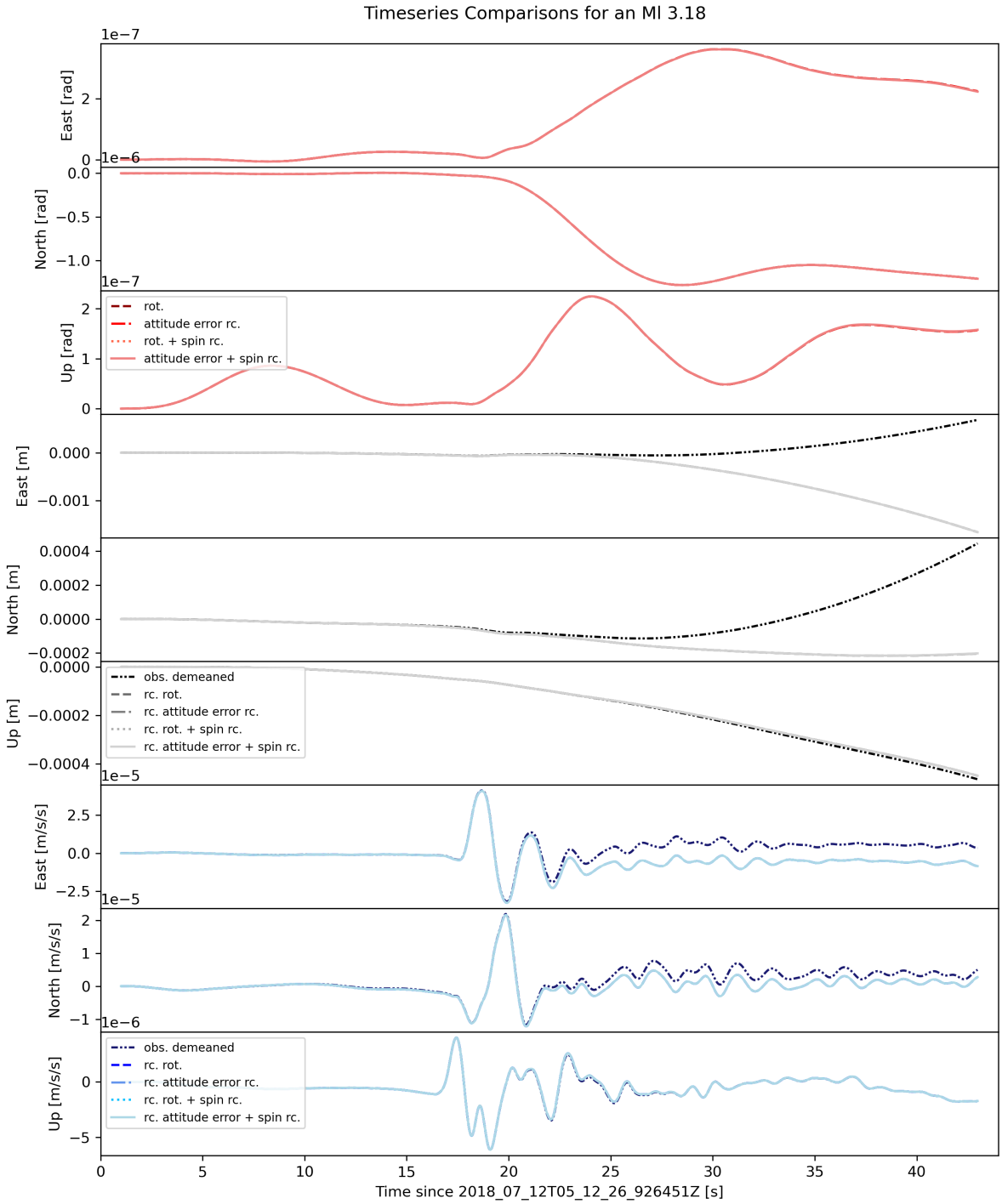

Figure 2 Recording of an earthquake with an Ml 3.18 at Kīlauea Caldera on 2018/07/12 using a lowpass filter. Top subfigures show the timeseries of the four versions of the angles; uncorrected and three rotation corrected versions. The middle subfigures show the displacement applying either demeaning or rotation correction using each of the four angles from above. The lowest subfigures show the same but for acceleration.

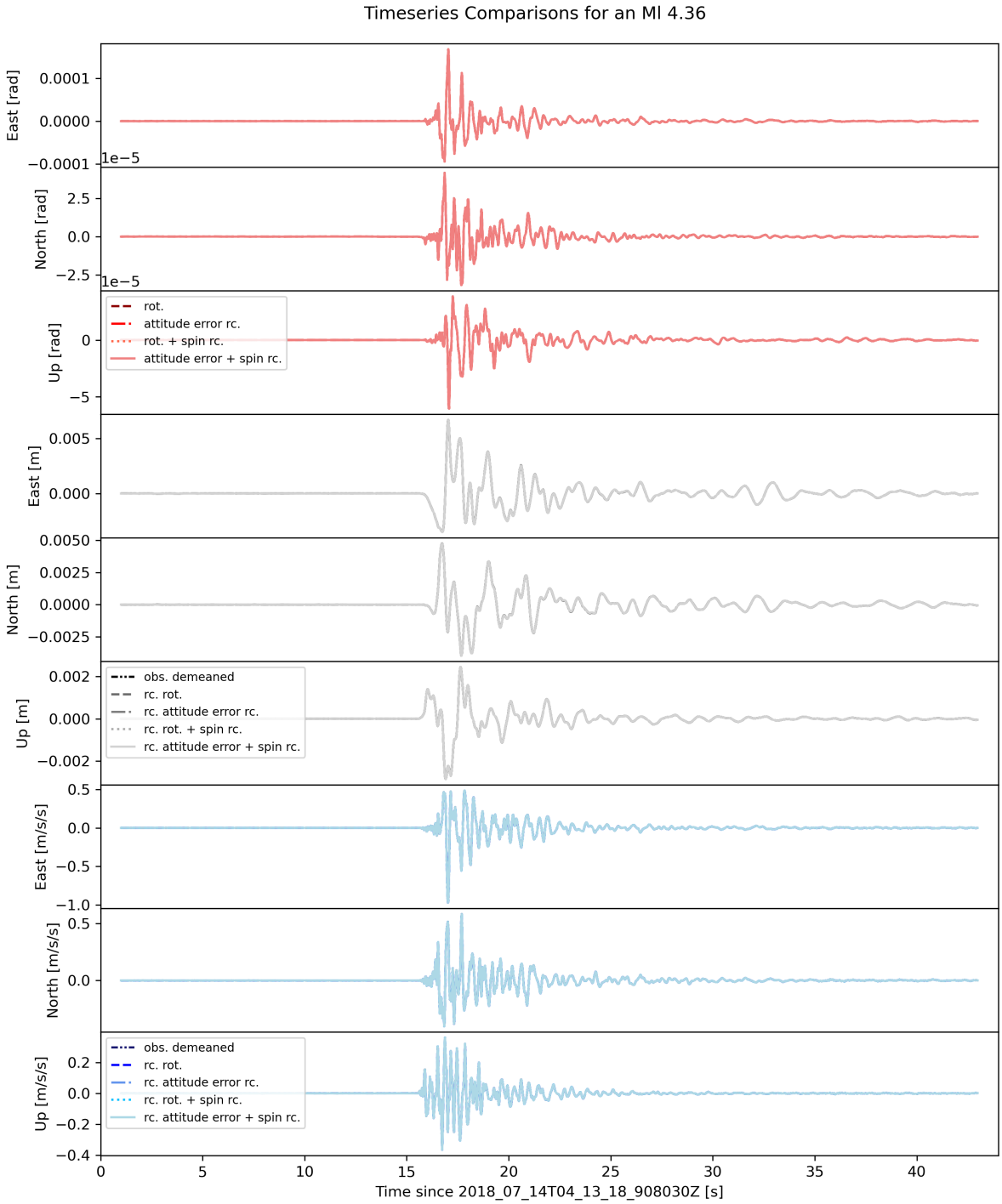

Figure 3 Recording of an earthquake with an Ml 4.36 at Kīlauea Caldera on 2018/07/14 using a highpass filter. Top subfigures show the timeseries of the four versions of the angles; uncorrected and three rotation corrected versions. The middle subfigures show the displacement applying either demeaning or rotation correction using each of the four angles from above. The lowest subfigures show the same but for acceleration.

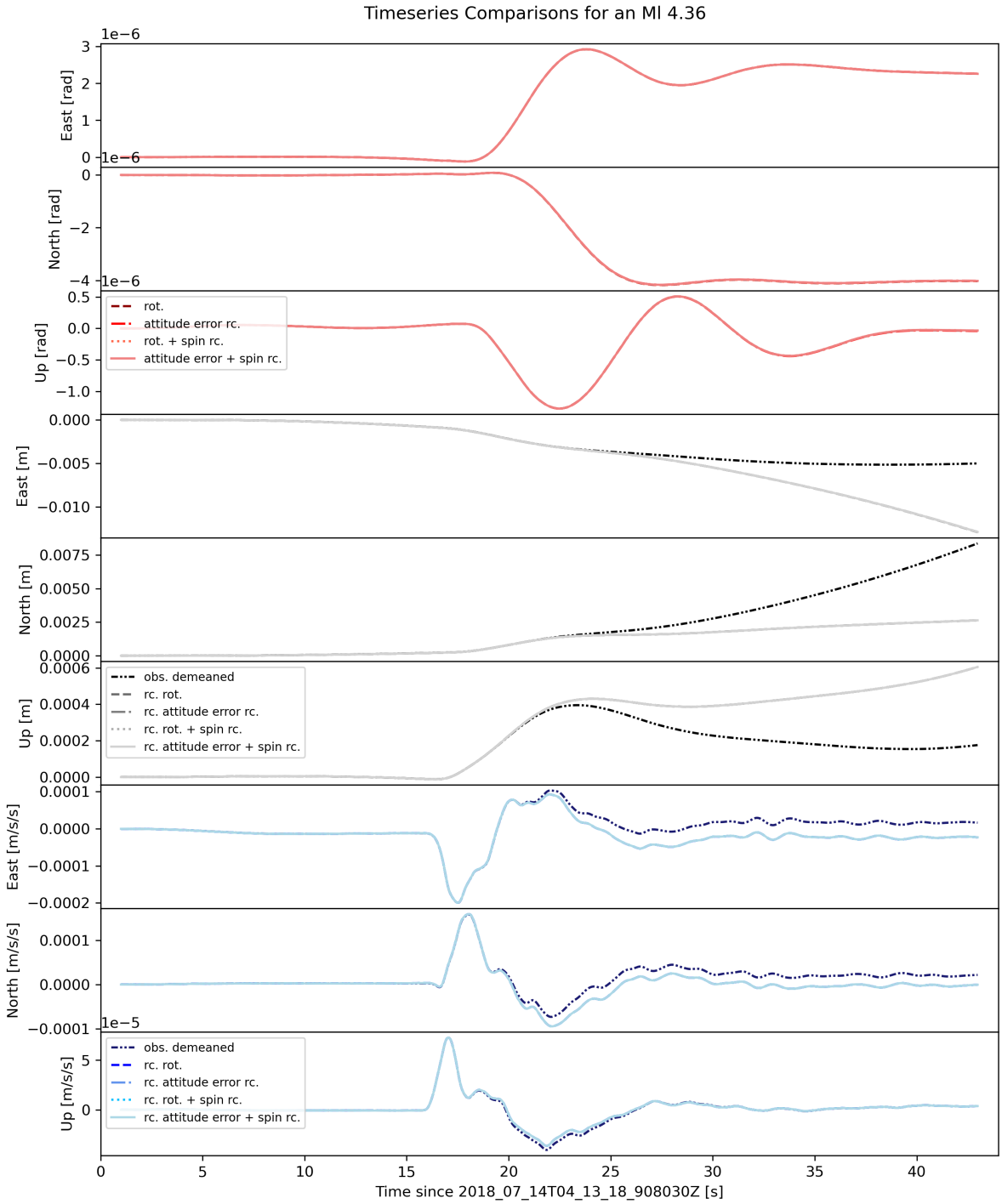

Figure 4 Recording of an earthquake with an Ml 4.36 at Kīlauea Caldera on 2018/07/14 using a lowpass filter. Top subfigures show the timeseries of the four versions of the angles; uncorrected and three rotation corrected versions. The middle subfigures show the displacement applying either demeaning or rotation correction using each of the four angles from above. The lowest subfigures show the same but for acceleration.

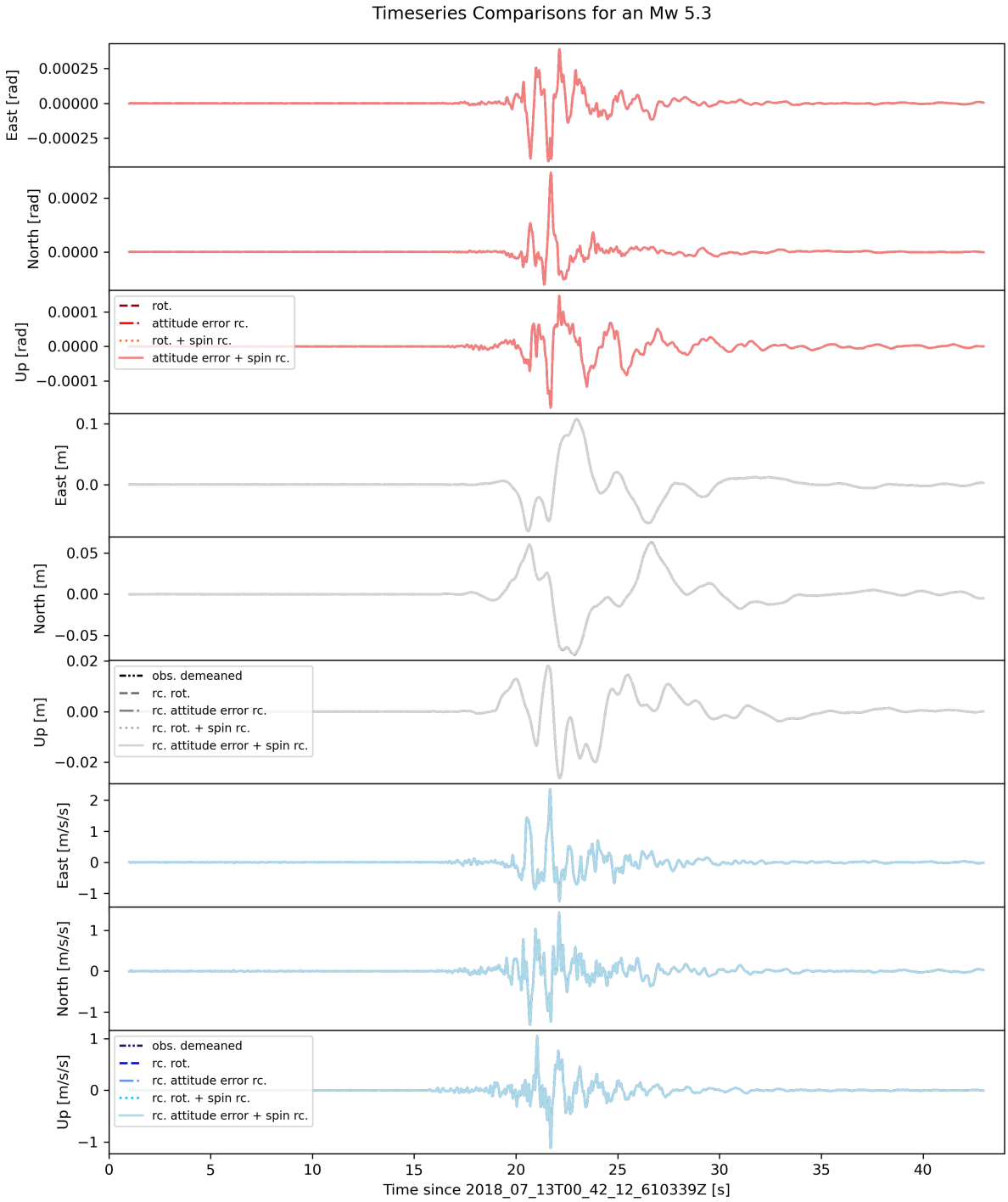

Figure 5 Recording of a summit collapse with an Mw 5.3 at Kīlauea Caldera on 2018/07/13 using a highpass filter. Top subfigures show the timeseries of the four versions of the angles; uncorrected and three rotation corrected versions. The middle subfigures show the displacement applying either demeaning or rotation correction using each of the four angles from above. The lowest subfigures show the same but for acceleration.

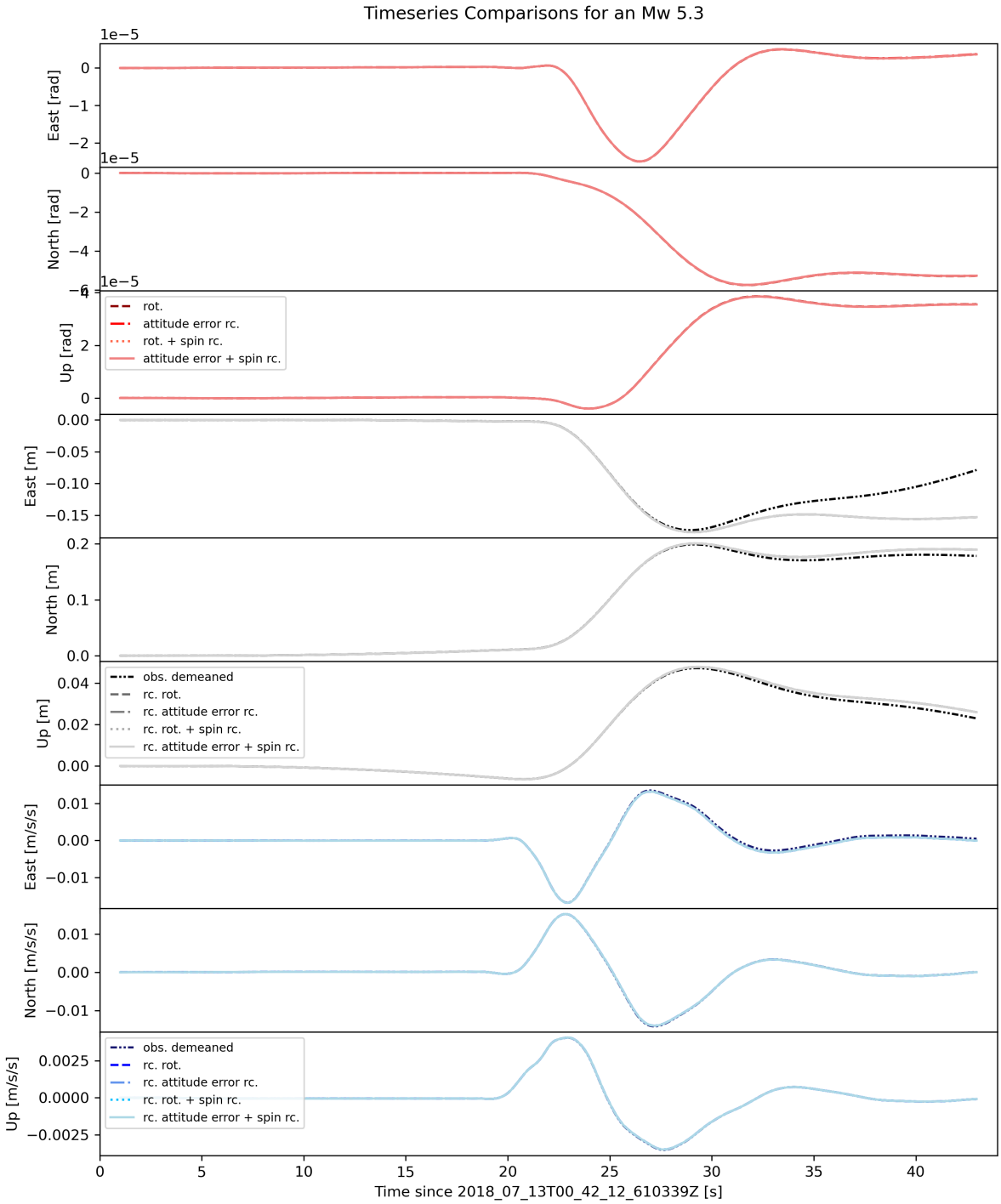

Figure 6 Recording of a summit collapse with an Mw 5.3 at Kīlauea Caldera on 2018/07/13 using a lowpass filter. Top subfigures show the timeseries of the four versions of the angles; uncorrected and three rotation corrected versions. The middle subfigures show the displacement applying either demeaning or rotation correction using each of the four angles from above. The lowest subfigures show the same but for acceleration.

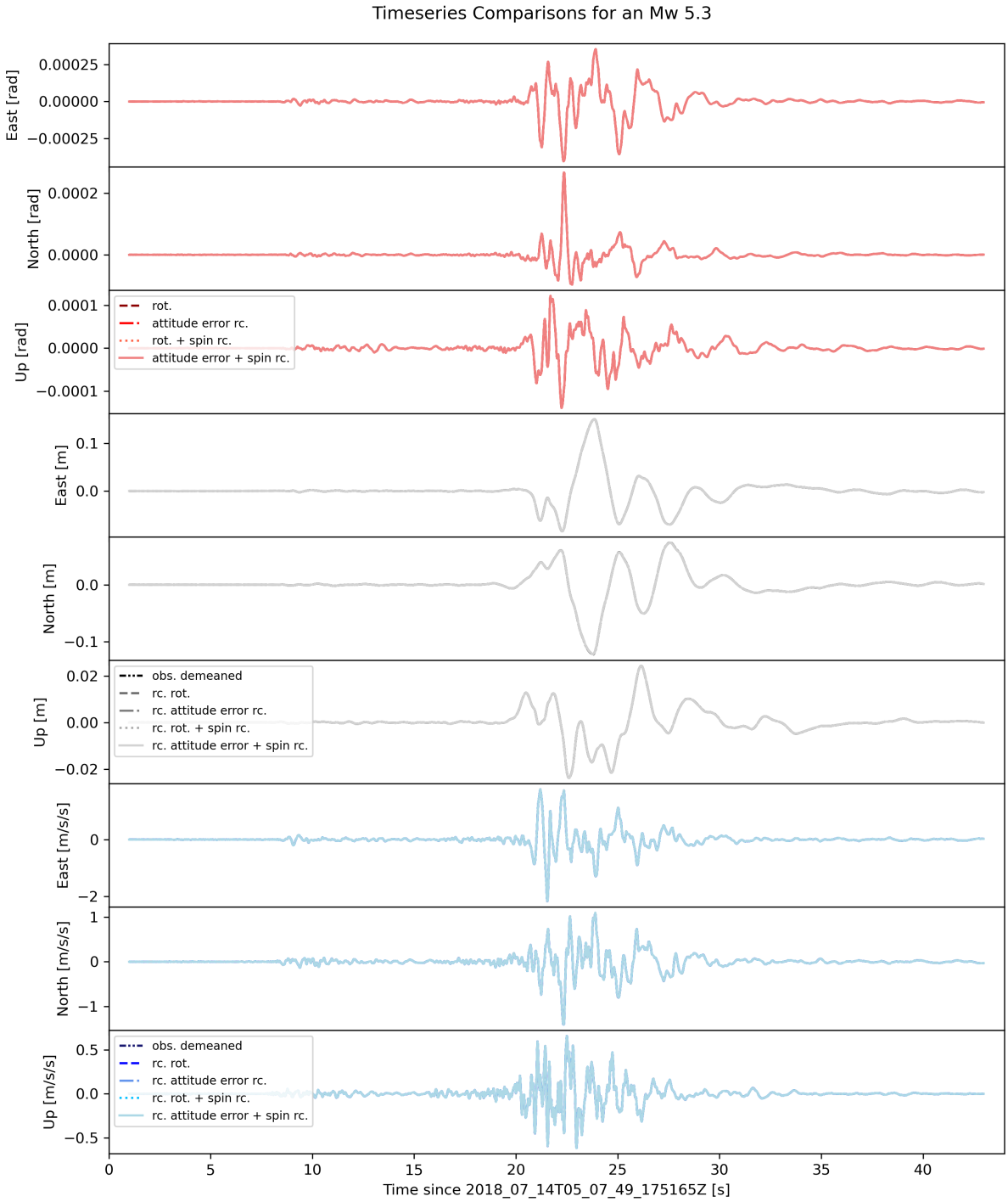

Figure 7 Recording of a summit collapse with an Mw 5.3 at Kīlauea Caldera on 2018/07/14 using a highpass filter. Top subfigures show the timeseries of the four versions of the angles; uncorrected and three rotation corrected versions. The middle subfigures show the displacement applying either demeaning or rotation correction using each of the four angles from above. The lowest subfigures show the same but for acceleration.

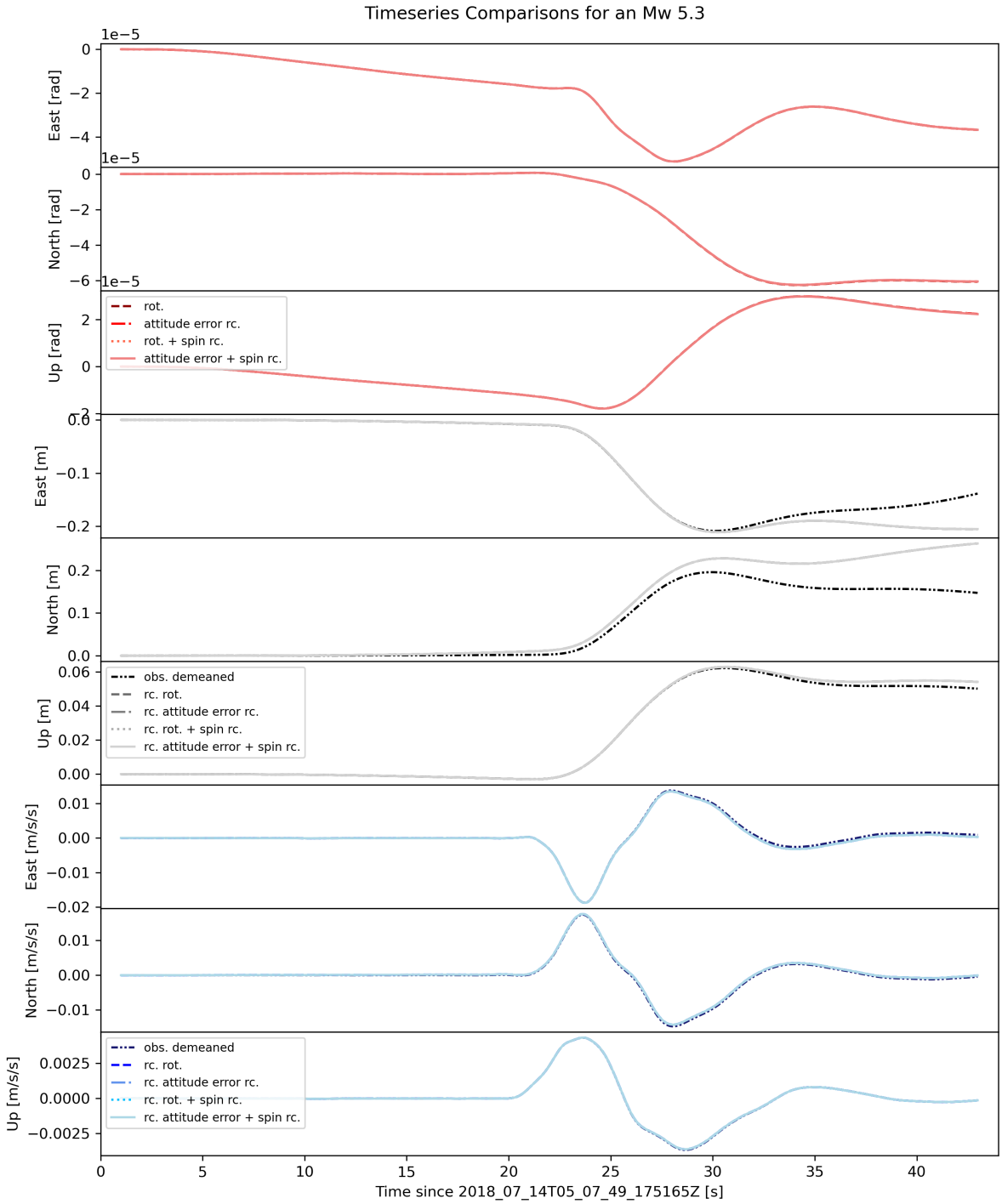

Figure 8 Recording of a summit collapse with an Mw 5.3 at Kīlauea Caldera on 2018/07/14 using a lowpass filter. Top subfigures show the timeseries of the four versions of the angles; uncorrected and three rotation corrected versions. The middle subfigures show the displacement applying either demeaning or rotation correction using each of the four angles from above. The lowest subfigures show the same but for acceleration.

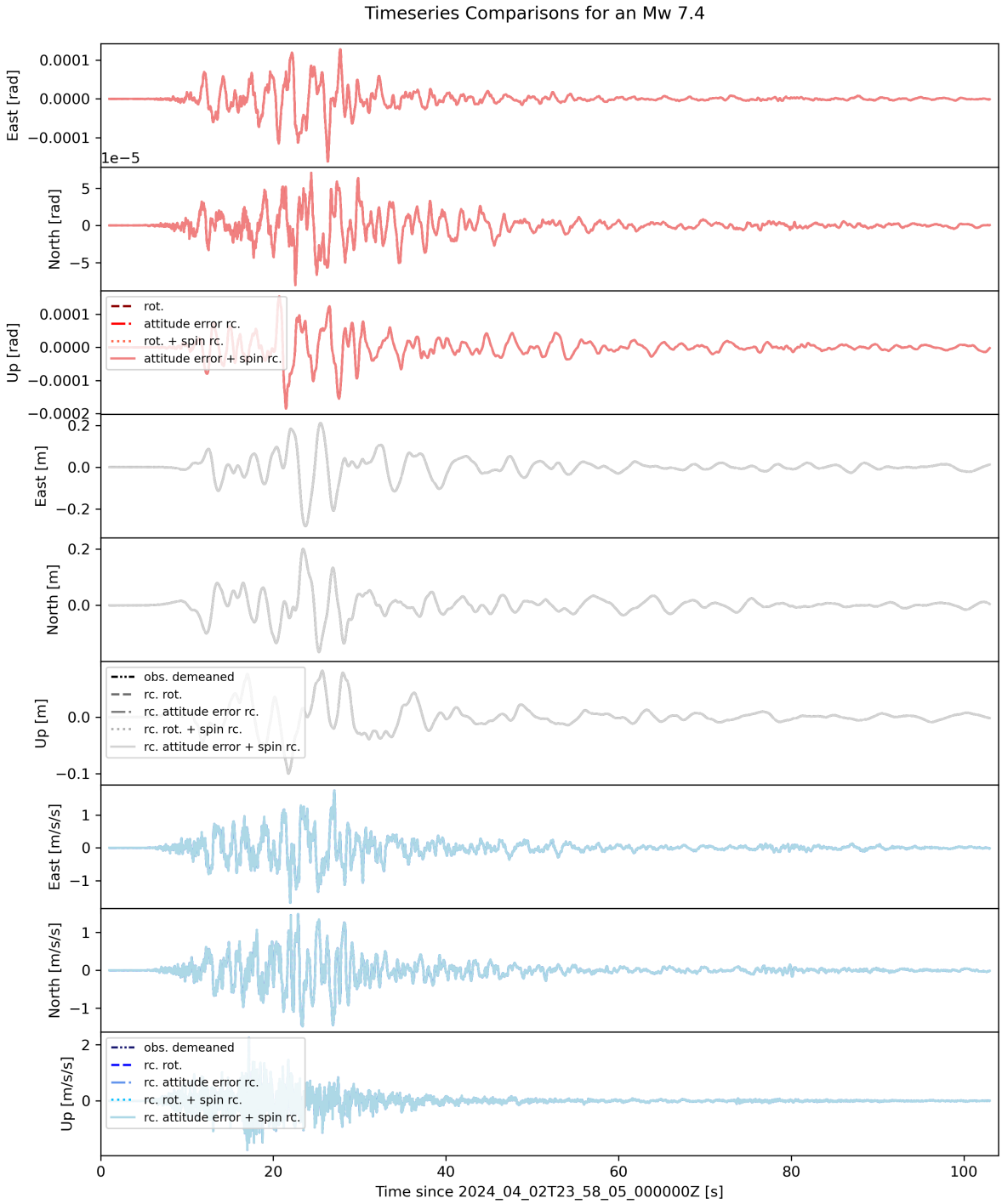

Figure 9 Recording of the Mw 7.4 earthquake in Taiwan on 2024/04/02 at station MDSA0 using a highpass filter. Top subfigures show the timeseries of the four versions of the angles; uncorrected and three rotation corrected versions. The middle subfigures show the displacement applying either demeaning or rotation correction using each of the four angles from above. The lowest subfigures show the same but for acceleration.

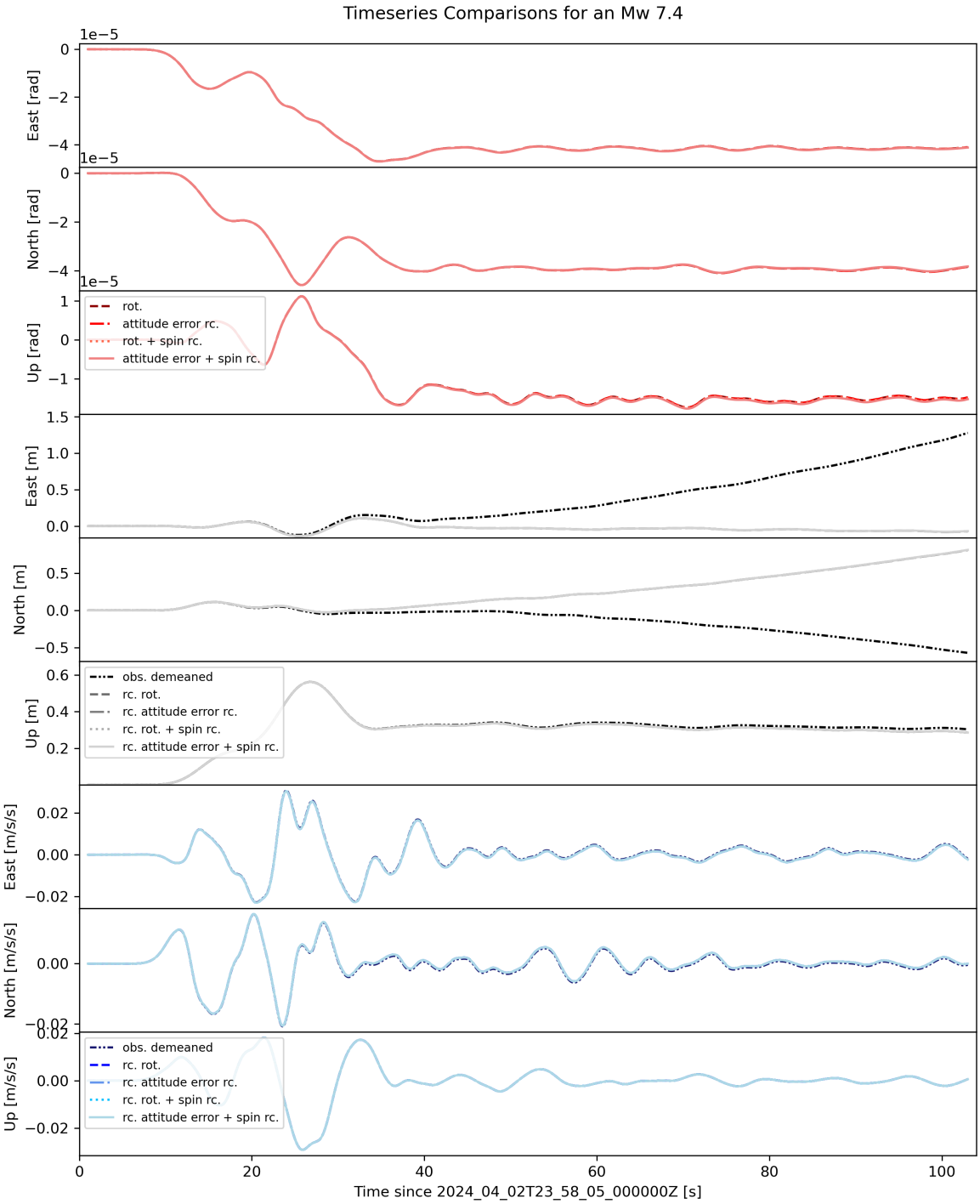

Figure 10 Recording of the Mw 7.4 earthquake in Taiwan on 2024/04/02 at station MDSA0 using a lowpass filter. Top subfigures show the timeseries of the four versions of the angles; uncorrected and three rotation corrected versions. The middle subfigures show the displacement applying either demeaning or rotation correction using each of the four angles from above. The lowest subfigures show the same but for acceleration.

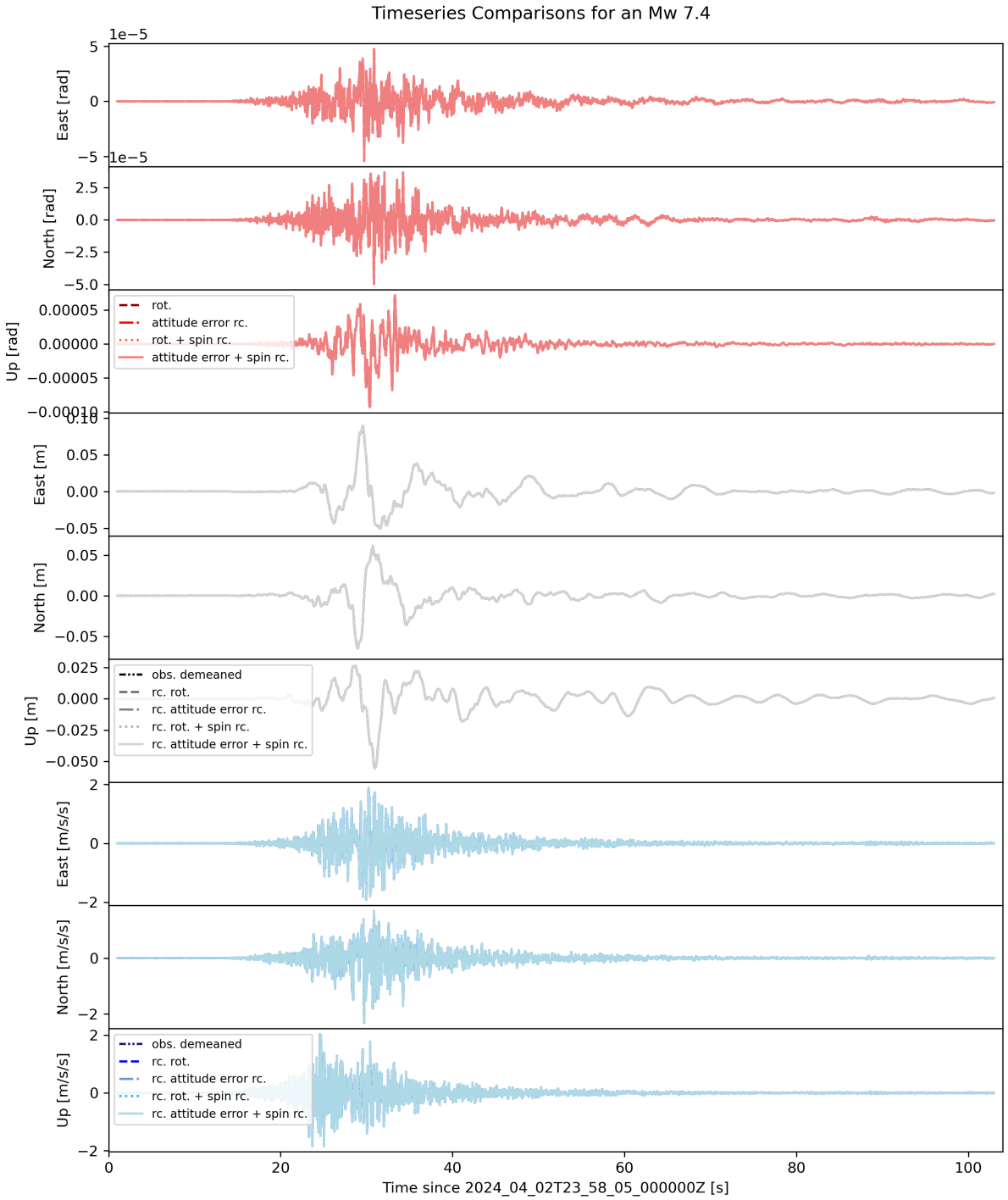

Figure 11 Recording of the Mw 7.4 earthquake in Taiwan on 2024/04/02 at station NA01 using a highpass filter. Top subfigures show the timeseries of the four versions of the angles; uncorrected and three rotation corrected versions. The middle subfigures show the displacement applying either demeaning or rotation correction using each of the four angles from above. The lowest subfigures show the same but for acceleration.

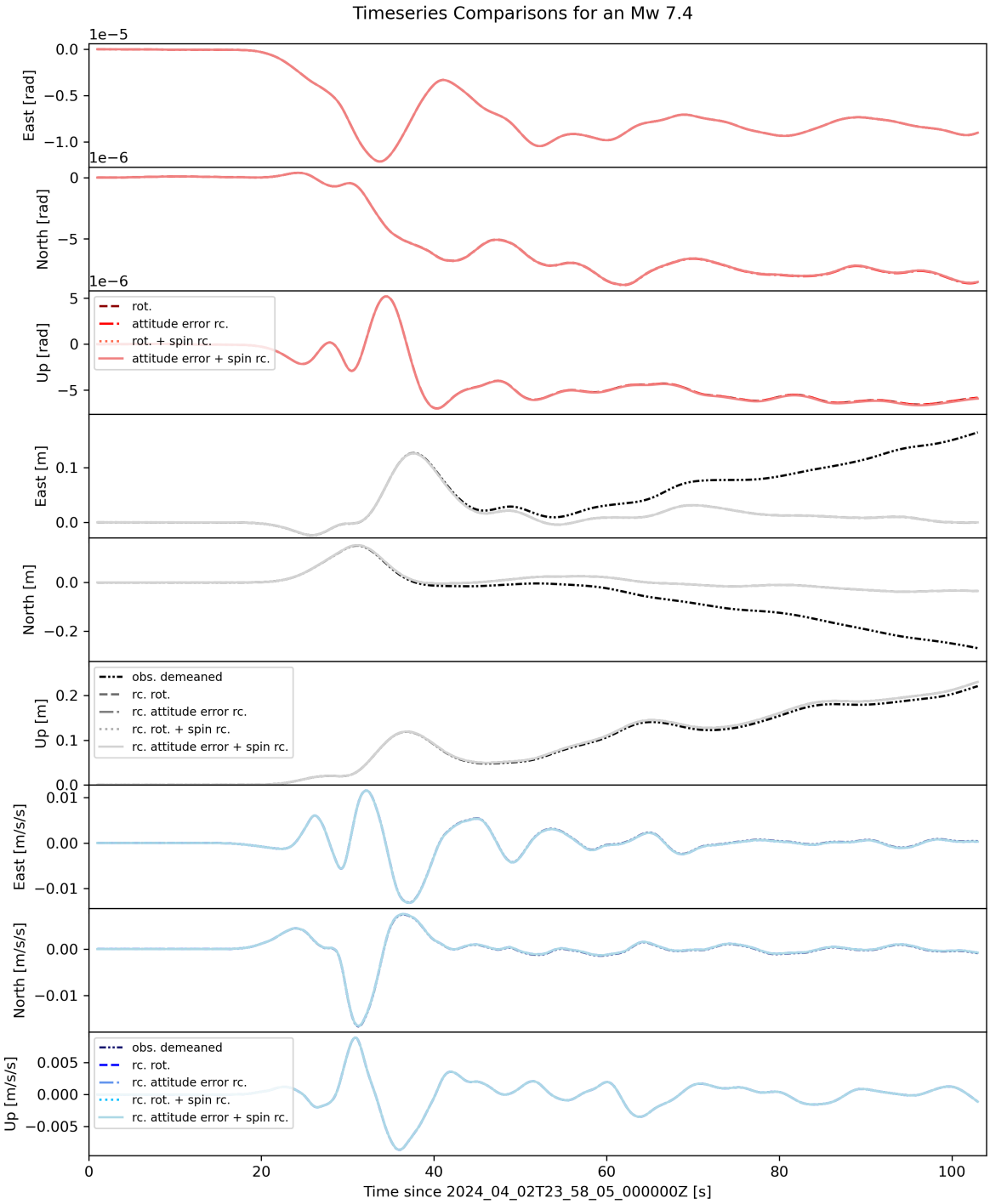

Figure 12 Recording of the Mw 7.4 earthquake in Taiwan on 2024/04/02 at station NA01 using a lowpass filter. Top subfigures show the timeseries of the four versions of the angles; uncorrected and three rotation corrected versions. The middle subfigures show the displacement applying either demeaning or rotation correction using each of the four angles from above. The lowest subfigures show the same but for acceleration.